

www.acsabm.org Article

Controlled Delivery and Photopatterning of Mechanical Properties in Polysaccharide Hydrogels Using Vanadium Coordination and Photochemistry

E. A. Kalani D. Edirisinghe, Carina Haddad, and Alexis D. Ostrowski*



Cite This: ACS Appl. Bio Mater. 2022, 5, 4827–4837



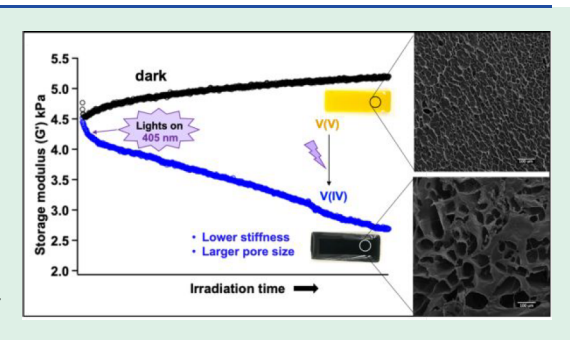
ACCESS I

Metrics & More

Article Recommendations

Supporting Information

ABSTRACT: Incorporation of the transition metal ion V(V) into hydrogels has been used to impart photoresponsive behavior, which was used to tune materials properties during light irradiation. The photoreaction in QHE-cellulose/agarose hydrogels coordinated with vanadium was evidenced by a clear color change of yellow to blue through a green intermediate. This color change was attributed to the reduction of V(V) to V(IV) as described in our previous work. A concomitant oxidative breakdown of the polysaccharide chain was noticeable upon the reduction of V(V) with a decrease in stiffness V(V) of the hydrogel material. This reduction of the metal ion and breakdown of polysaccharide chain induced irreversible changes in the microstructure of the hydrogel, enabling the controlled delivery of V(V) and/or encapsulated



cargo. Scanning electron microscopy studies showed an increase in pore sizes and guest cavity formation during irradiation. In addition to the significant drop in mechanical properties like storage and loss modulus in the gel materials, a viscosity drop in the polymer solution was observed through irradiation, indicating breakdown of the polysaccharide chain. A photomask can be used to create discrete patterns on these materials upon irradiation.

KEYWORDS: vanadium coordination, photoresponsive hydrogels, controlled release, polysaccharide gels, metallosupramolecular gels

■ INTRODUCTION

Due to their tunable properties, hydrogels are versatile materials that are functional in a wide range of applications from wastewater treatment, 1,2 tissue engineering, 3,4 regenerative medicine, 5,6 and drug delivery 7,8 to soft robotics. 9,10 Hydrogels are three-dimensional polymer networks that are typically cross-linked with hydrogen-bonding interactions and are capable of absorbing and retaining large amounts of water. Incorporation of metal ions has been used to create new dynamic covalent bonding interactions that can lead to more mechanically robust hydrogels. 12-14 For example, we have shown that coordination of vanadium(V) in polysaccharide materials results in enhanced water stability due to the metal coordination. 15 When a metal ion (e.g., V(V) or Fe(III)) is incorporated into the polymeric system, the oxidation state of the metal ion and concomitant functional groups can be altered upon irradiation, which ultimately changes the properties of the overall material matrix. 16 In previous work, we have demonstrated how Fe(III) coordination in polysaccharide hydrogels makes the materials photoresponsive, and this photoresponsive behavior results in tuning of the properties of the gel during light irradiation because of the change in oxidation state to Fe(II) and the photochemical reaction that involves the polymer backbone.^{3,17} Vanadium is known to have many different stable oxidation states, 18 and depending on the valence state of vanadium ion, discrete colors

like violet, green, blue, and yellow can be seen for V(II), V(III), V(IV), and V(V) respectively. 19 Vanadium shows up in marine environments, and it is hypothesized that one of the roles of V in ascidians is to act as a cross-linker to tune the mechanical properties, similar to Fe(III) coordination in mussels.²⁰ Vanadium compounds are used as antidiabetic agents and insulin mimetics.^{21,22} A rapid growing area in drug delivery research is the use of ionic polysaccharides to release drugs selectively in target organs in response to external stimuli.²³ Delivery of vanadium complexes in ionic polysaccharides by means of biological reductants was reported.²⁴ However, light is a nearly ideal stimulus for molecular systems with high precision in wavelength and intensity without contamination of the target.²⁵ Hence, photoregulated drug delivery is an emerging therapeutic platform. 26,27 In a previous study, the photochemical transformation of V(V) tartrate clusters into V(IV) tartrate was described. 28 This unique coordination chemistry provided inspiration for the design of a

Received: June 7, 2022 Accepted: August 9, 2022 Published: September 23, 2022





novel vanadium-coordination hydrogel that would feature tunable properties and photoreactivity. Thus, we report here photoresponsive V(V) hydrogels for controlled delivery without using any sacrificial reductant. We introduced V(V) coordination cross-links into polysaccharide hydrogels, where these cross-links were photoresponsive and the properties of the hydrogel could be tuned during light irradiation since V(V) was photochemically reduced to V(IV) with oxidation of the polymer matrix.

For the hydrogel formulation, we chose agarose and cellulose for the backbones. Agarose is a biocompatible polysaccharide having self-gelling properties²⁹ and is widely used as a three-dimensional (3D) scaffold.³⁰ Cellulose is biocompatible^{31,32} and the most abundant natural biopolymer on earth, with many attractive physical properties such as high Young's modulus for a single fibril, high degree of crystallinity (89%), high degree of polymerization (14 400), and high specific surface area (37 m² g⁻¹).³³ Cellulose can be functionalized to contain donor groups, including alcohol and carboxylate, affording acceptable candidates for the adsorption of heavy metals and dyes.^{34,35} Quaternary ammonium monomers with cationic groups are widely used for superabsorbent hydrogels.³⁶ Because of the quaternary ammonium cationic heads, these hydrogels favor absorption of negatively charged molecules and are also responsive to ionic strength and pH.³⁷

Transformation of cellulose and its derived carbohydrates into formic and lactic acids is reported upon reduction of V(V)to V(IV). 38,39 Thus, we disclose a "two birds, one stone" approach to incorporate vanadium using quaternary ammonium coordination moieties to the cellulose network (QHEcellulose) to ensure better coordination and solubility, where photoexcitation will lead to the reduction of V(V) upon concomitant oxidative breakdown of cellulose in the absence of a sacrificial reductant. This will open the possibility to use these hydrogels as a biocompatible medium for the photoinduced release of V(IV) and/or encapsulated cargo. Similarly, light can be used to create discrete patterns on the hydrogel materials as gradients in stiffness and elasticity. By photopatterning, we can create mechanical grooves to code the functionality within the same hydrogel. Furthermore, based on the reverse oxidation of V(IV) to V(V), these materials can be recycled and reused for sustained release.

EXPERIMENTAL SECTION

Materials. Ouaternized hydroxyethyl cellulose ethoxylate (OHEcellulose) (lot no. MKBH7404V), low-viscosity alginic acid sodium salt from brown algae (lot no. SLCH7413), pectin from citrus peel (galacturonic acid \geq 74.0%, dried basis, lot no. SLCG1374), sodium metavanadate (NaVO₃) (anhydrous, purity \geq 98%), Folic acid (purity \geq 97%, lot no. 070M1627V), deuterium oxide (D₂O) (99.99%), and deuterium chloride (DCl) (35 wt % in D2O, ≥99 atom % D) were purchased from Millipore Sigma Chemical Company. Electrophoresisgrade ultrapure agarose (lot no. 30819) was obtained from Bethesda Research Laboratories, Inc. Concentrated hydrochloric acid (HCl) (38% assay) and concentrated nitric acid (HNO₃) (70.0% assay) were purchased from EMD Millipore Corporation. Potassium bromide crystals were purchased from Baker & Adamson Reagents, General Chemical Division. All chemicals were of the highest purity grade and were used as commercially obtained. All aqueous solutions, including metal solutions, polymer solutions, and HCl solutions, were prepared with deionized water.

Choosing the Photoactive Polysaccharide Component. QHE-cellulose, pectin, and alginate were tested as the photoactive component. Hydrogels were formed with 1% w/v polysaccharide and

1% w/v agarose as described below. Each hydrogel was soaked in 25 mM $\,$ NaVO $_3$ solution and irradiated under 405 nm light at an irradiance power of 314 mW/cm² for 3 h as described later to craft the photosensitivity of the gels (Figure S2). QHE-cellulose/agarose—V(V)-coordinated hydrogels showed the most intense yellow color, indicating the best coordination, least leaching, and the best photosensitivity. Thus, QHE-cellulose was preferred as the photoactive polysaccharide component, and QHE-cellulose/agarose hydrogel was chosen for the study.

Synthesis of 1% w/v QHE-cellulose/1% w/v Agarose Hydrogels. To determine the best hydrogel preparation method, several trial-and-error preparation methods were carried out. This method minimized the air bubble formation inside the gels. In this method, 1% by weight agarose (0.1 g) was added to 10 mL of roomtemperature water in a 100 mL centrifuge tube with stirring in a vortex mixer. Additional vortexing was done for 15 s at high speed with the cap on until the polymer was initially mixed without clumping up. The mixture was heated at 96 °C for 7 min in the water bath with stirring at 450 rpm using a magnetic stirrer with the cap loosened. Then 1% by weight QHE-cellulose (0.1 g) was added in the same way with vortexing, and the mixture was heated at 96 °C for another 6 min similarly until both polymers were well-dissolved. The solutions were centrifuged hot at 1000 rpm for 2 min. The tubes were kept back in the water bath for an additional 2 min without stirring. The mixtures were then poured into Teflon elastomeric molds of 70 mm length, 70 mm width, and 1.95 mm thickness. The hydrogels were allowed to cure for 30 min at room temperature, carefully taken out of the molds, and soaked in a 25 mM aqueous NaVO3 solution at pH 4 as acidified with HCl. The hydrogels were soaked for 3 h under dark conditions. A fresh metal solution was used every time. The gels were then rinsed with water three times to wash away the unreacted and excess polymer and metal ion.

pH Dependence of the Hydrogels. The pH dependence of the vanadium-QHE-cellulose coordination and photochemistry was studied in solution. NaVO3 (5 mM) was dissolved in 1% w/v QHE-cellulose solution, and a series of solutions with different pH were prepared. The pH was varied from 1.63 to 9.95 (approximately from 1 to 10), and then the range was narrowed from 2.50 to 8.50, where the most noticeable color change was observed (Figure S3). Two tests were carried out for each pH. Each system was irradiated at 405 nm with a power of 314 mW/cm² for 12 h, and the control was kept in the dark. The irradiated systems were kept in the dark for 48 h, and the backward oxidation reaction was also monitored over this period. Similarly, the QHE-cellulose/agarose hydrogels as prepared above were then studied at a series of pH values (Figure S3). The hydrogels were soaked in 25 mM NaVO₃ solutions at pH 3.37, 4.02, 5.03, 6.75, and 8.03 for 3 h and irradiated at 405 nm and 314 mW/ cm² for 12 h. The irradiated hydrogels were kept in the dark for up to 48 h, and the backward oxidation reaction was observed. The photoreaction at each pH was monitored with a dark control. On the basis of the intensity of the V(V) coordination complex and the reversibility of the photoreaction, the experimental pH was chosen as 4 (Figure S3-S4).

Photochemical Treatment of Hydrogels. By immersion of the QHE-cellulose/agarose hydrogel in a V(V) solution, a photoresponsive material was created. To induce the irreversible mechanical and structural changes, the coordinated hydrogels were irradiated at 405 nm and 314 mW/cm² using an LED lamp (Thorlabs, part no. M405 L3, spot diameter 5.8 cm). A continuous significant color change from yellow to green to blue was observed in the hydrogels. Gradual leaching of the photoproduct was observed with irradiation.

Rheological Measurements. To characterize the mechanical properties, the hydrogels were punched to obtain discs with a diameter of 8 mm. The punch-cut gel discs were equilibrated in aqueous solutions before analysis. The study of mechanical properties was performed in a TA Instruments Discovery HR-2 hybrid rheometer equipped a Peltier plate with a parallel-plate geometry. The gels were irradiated under a 405 nm LED lamp as above. For the dynamic shear measurements for storage modulus, the axial force was

kept at 0.1 N, and the samples were sheared at a fixed frequency of 10 Hz while sweeping the strain from 1 to 100%.

Viscosity of the Vanadium–QHE-cellulose Coordination. For the viscosity measurements, 10 mM NaVO $_3$ in 2% QHE-cellulose solution at pH 4 was used. This system had a decent viscosity at the beginning. The solution was irradiated over time, and the viscosity drop was monitored using a 50 mm 2° cone plate in the TA Instruments DHR-2 Rheometer. Approximately 0.6 mL of the sample was added between the plates when the gap was 500 μ m and the initial velocity was 2.0 rad/s. The shear rate was 1–100, and the soak time was maintained at 30 s at 20 °C.

Scanning Electron Microscopy (SEM). Hydrogel samples were freeze-dried with liquid nitrogen, lyophilized, and sputter-coated with Au/Pd. SEM images were collected on a Hitachi S2700 scanning electron microscope at a voltage of 12 kV.

Ultraviolet–Visible Spectroscopy (UV–Vis). The absorbance spectra were measured using a Shimadzu UV-2600 spectrophotometer with a resolution of 1.0 nm. For absorbance measurements of V(V)-coordinated polysaccharide solutions, 2 mL solutions of 0.05% w/v QHE-cellulose mixed with 0.5 mM NaVO $_3$ at pH 4 were prepared in the dark and irradiated at 405 nm as above. Absorbance spectra upon each irradiation time were recorded.

Leaching Studies. To determine the leaching profile upon irradiation, the absorbance of a 2 mL aqueous solution above an 8 mm gel disc was measured using a UV—vis spectrophotometer after each irradiation.

Fourier Transform Infrared Spectroscopy (FTIR). Hydrogel samples were freeze-dried with liquid nitrogen, lyophilized, and placed on a holder to collect transmission spectra in a Jasco FTIR-4000 spectrometer. For the irradiation experiment, the aerogel was fixed to the sample holder and irradiated at 405 nm and 314 mW/cm² without changing the exposure region. QHE-cellulose was characterized by a KBr pellet prepared using a dry pellet pressing die set and placed in the sample holder.

Thermogravimetric Analysis (TGA). Freeze-dried and lyophilized hydrogel samples were used in the TGA analysis. A mass of 4–10 mg from each sample was placed in a ceramic crucible. The analysis was done throughout the temperature range of 25–1000 $^{\circ}\text{C}$ at a heating rate of 10 $^{\circ}\text{C/min}$ using a HITACHI STA7200 thermal analysis system. The analysis was done in air with an air flow rate of 200 mL/min.

Folic Acid-Encapsulated Beads and Photorelease. A mass of 8 mg of folic acid was dissolved in 1 mL of 1% w/v QHE-cellulose/1% w/v agarose polymer solution. This solution was slowly added dropwise from a syringe with a 25 gauge needle to a 25 mM NaVO3 solution at pH 4 to make the folic acid-encapsulated V(V)-QHE-cellulose/agarose gel beads. The spherical-shaped beads were stored in the setting solution for 3 h under dark conditions to allow coordination with the metal and washed three times in distilled water to remove unreacted substances. To show light-triggered release, the beads loaded with folic acid (12 beads each) were placed in a 1 cm path length quartz cuvette, and 2 mL of distilled water was added. The beads were irradiated at 405 nm as above. The absorbance of the release medium above the beads was measured after each irradiation. The increase in absorbance at 268 nm was considered for the screening.

Diffuse Reflectance Spectroscopy. Hydrogel samples were cut into small rectangular strips with dimensions of approximately 3 cm × 1.3 cm, and the color change upon irradiation was monitored using diffuse reflectance spectroscopy. A halogen light source (HL-2000-FHSA, Ocean Optics) was used to shine white light on the sample through an optical fiber, and the reflected light was detected by an Ocean Optics Flame miniature spectrometer. The gel sample was blotted dry, kept on a white paper, and covered with a black paper when placed on white light to ensure reflection from the sample. OceanView spectroscopy software was used to obtain the spectra of percentage reflection against wavelength.

Swelling Experiments. The hydrogel samples were punch-cut to obtain 8 mm diameter gel discs, which were irradiated in water under a 405 nm LED light at an irradiance power of 314 mW/cm² for

different intervals. Specimens were air-dried for 24 h and then stored in a desiccator. For the swelling study, five discs per each irradiation were soaked in 10 mL of deionized water for 24 h. Fully swollen gel discs were wiped with a Kimwipe, and the swelling percentage was calculated using the equation

swelling percentage =
$$\frac{m_{\rm w} - m_{\rm o}}{m_{\rm o}} \times 100\%$$

where $m_{\rm w}$ is the weight of the soaked disc and $m_{\rm o}$ is the weight of the air-dried disc. Swelling of the oxidized gel discs was determined after the irradiated gel discs were stored for 7 days in deionized water, letting V(IV) to oxidize back to V(V). The experiment was performed at room temperature (25 °C).

Inductively Coupled Plasma Optical Emission Spectroscopy (ICP-OES). Freeze-dried and lyophilized hydrogel samples were used in the ICP-OES analysis. The samples (5 mg each) were added to 2 mL of a concentrated HNO₃/HCl mixture. The polysaccharide matrix was digested with shaking on a mechanical shaker for 12 h. The acid-digested mixture was diluted with 5 mL of 3.5% HNO₃ prepared with nanopure water. Samples were analyzed using a Thermo element iCAP 6500 series ICP emission spectrometer. Calibration standards were prepared using the 1000 ppm vanadium analytical reference standard from Lab Standards, LLC (lot no. 2101830) in 3.5% nitric acid. All of the calibration standards, the check standard (100 ppm) prepared separately from the calibration standards, the blank, and the samples were prepared in 3.5% HNO₃ solution. The vanadium content in each sample was measured using a calibration curve with emissions measured at 294.4, 406.8, and 440.2 nm, respectively.

Nuclear Magnetic Resonance Spectroscopy (NMR). 1 H NMR spectra were recorded on a Bruker Avance III 500 MHz spectrometer. V-QHE-cellulose solutions were prepared in D_2O and acidified with DCl, and NMR spectra were obtained before and after irradiation.

■ RESULTS AND DISCUSSION

We utilized agarose and quaternized cellulose (QHE-cellulose) to create hydrogel materials that coordinate to V(V). Agarose was used as the structural polysaccharide polymer that gives mechanical stability and gelling properties to the material. We introduced a responsiveness that was not present in pure agarose hydrogels and was due to the quaternary ammonium functional groups in the cellulose. QHE-cellulose has a high affinity for metal ions 41,42 and therefore coordinates to the vanadium ions. After QHE-cellulose/agarose hydrogels were immersed in a VO $_3^-$ solution to coordinate the vanadium(V) ions into the material, the hydrogels were irradiated at 405 nm at a power of 314 mW/cm² to induce irreversible structural and mechanical changes (Figure 1).

The porous structure of the hydrogel hosts hydrophilic groups such as -COOH, -OH, -NH₂, etc., which enable the adsorption and retention of water and metal ions.⁴³ The adsorption of heavy metals by QHE-cellulose-based hydrogels typically occurs through different types of interactions, such as hydrogen bonding, coordination cross-linking, and electrostatic interactions where anionic molecules are attracted by the cationic ammonium groups. ^{1,36,37,44} QHE-cellulose was chosen as the photoactive polysaccharide component for this study based on the better coordination and better photoresponsiveness with VO₃⁻ at pH 4 compared to pectin and alginate in the respective agarose hydrogels (Figures S1 and S2). QHEcellulose provided strong enough coordination with the V(V)moieties, presumably VO₃-, to enable stronger coordination of V(V) compared with V(IV), which is formed after the photoreaction. The excellent adsorption capacity of QHEcellulose derivatives is associated with the nature and amount of grafted groups on the polysaccharide backbone.³⁴ Thus, we anticipate that the unique coordination of QHE-cellulose over

ACS Applied Bio Materials www.acsabm.org Article

2.5

Control 0

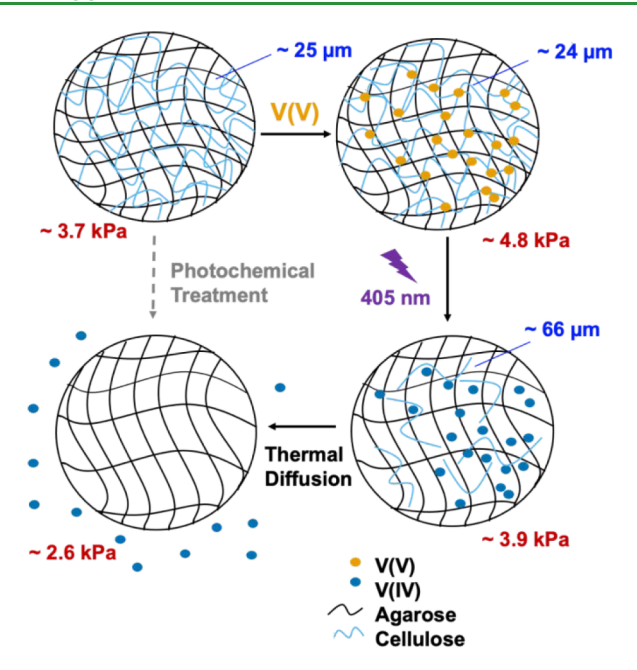


Figure 1. Schematic representation of the overall treatment of QHE-cellulose/agarose hydrogels with V(V) coordination and then photochemical treatment. The average pore diameters (in μ m) as measured by SEM and ImageJ software are stated in blue, and the storage moduli (in kPa) as measured by dynamic shear experiments are stated in red. The data correspond to 3 h of irradiation with 405 nm light at 314 mW/cm². A complete experimental data set is presented in Table S1.

pectin and alginate is due to the quaternary ammonium functional groups (Figure S1).

The interaction of the hydrogels with vanadium(V) was evidenced by the color change from colorless to bright yellow. The photoreaction was evidenced by a prominent color change from yellow to blue through a green intermediate (Figure 2A). This color change is attributed to the reduction of V(V) to V(IV) as described in our previous work.²⁸ With the introduction of vanadium ions, quaternary ammonium and other hydrophilic groups in polysaccharide matrix can coordinate with the metal. This results in new cross-links and an increase in the storage modulus (Figure 2B). Pure QHE-cellulose/agarose gels show less elasticity, which is attributed to the absence of the V(V) coordination crosslinks (Table S1). The photoresponse of the hydrogels under a 405 nm LED lamp showed a significant drop in storage modulus (Figures 2B and S6). This can be explained by the reduction and leaching of the metal ions and possible breakdown of cellulose chains followed by changes in the dynamics of the V coordination interaction now that it is V(IV). The loss modulus (E'') also showed a drop upon irradiation, indicating the decreased viscous dissipation of energy (Table S1). Significant changes in color were observed, and the color change was accompanied by the drop in the storage modulus (Figure 2A). The gradual color change through the gel was vibrant in the lateral views of the 8 mm gel disc (Figure S7). With extensive irradiation, total loss of the color was observed, which resulted a transparent gel at 24 h of irradiation (Figures 2A and S7). This was attributed to the complete leaching of the reduced metal V(IV) to the aqueous environment upon irradiation. As detailed later, the resulting material after prolonged irradiation was primarily agarose, and we attribute this to the oxidative breakdown of QHE-cellulose.

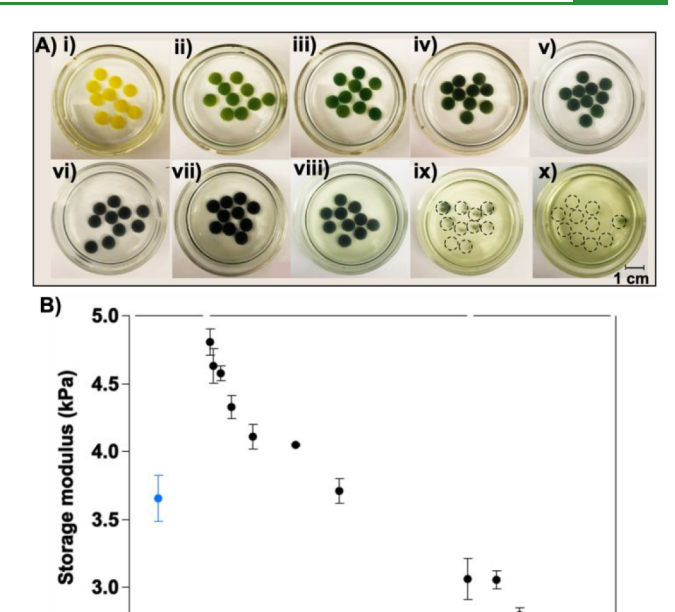


Figure 2. (A) Color change of punch-cut QHE-cellulose/agarose–V gel discs upon irradiation: (i) gel discs before irradiation; (ii) t=5 min of irradiation; (iii) t=15 min of irradiation; (iv) t=30 min of irradiation; (v) t=60 min of irradiation; (vi) t=120 min of irradiation; (vii) t=180 min of irradiation; (viii) t=360 min of irradiation; (ix) t=720 min of irradiation; (x) transparent gel discs at t=1440 min of irradiation. (B) Evolution of the storage modulus of QHE-cellulose/agarose–V gel discs upon irradiation at 405 nm and 314 mW/cm². The control is the QHE-cellulose/agarose gel without V coordination.

200

Time of irradiation (min)

300 400 800 1200

100

Even though light irradiation can create irreversible changes to the mechanical properties of the gels, the color response was reversible at any point of irradiation. Complete reversible color change from green to yellow as well as blue to yellow was observed when the irradiated gels were stored in the dark for 36-48 h, but the intensity of the yellow color corresponded to the leaching (Figure S8A). The reversible color response was monitored over three cycles in gel irradiated for 180 min until the metal was fully leached out from the material (Figure S8B). This color change was attributed to the reverse oxidation of V(IV) to V(V). 28,45 However, our study primarily focuses on the irreversible photoresponse on the hydrogel material, which will be discussed in detail.

The bulk mechanical property changes were consistent with the irreversible changes in the microstructure of the hydrogel during the photoreaction. The microstructure of the hydrogel upon irradiation was examined by scanning electron microscopy. Significant changes in surface texture and pore diameter were observed after light irradiation. QHE-cellulose/agarose hydrogels (control) showed a nonporous surface and a porous interior (Figures 3 and 4). Upon coordination of the metal, the interior changed to a more organized honeycomblike structure (Figure 4A), which was attributed to the new dynamic V(V) coordination interactions in the gels. Photochemical treatment caused a significant increase in the pore size of the hydrogel, almost 3 times in 3 h of irradiation (Figure 4B). We attribute this to the changes in cross-link density of the material followed by the degradation of cellulose. Novel

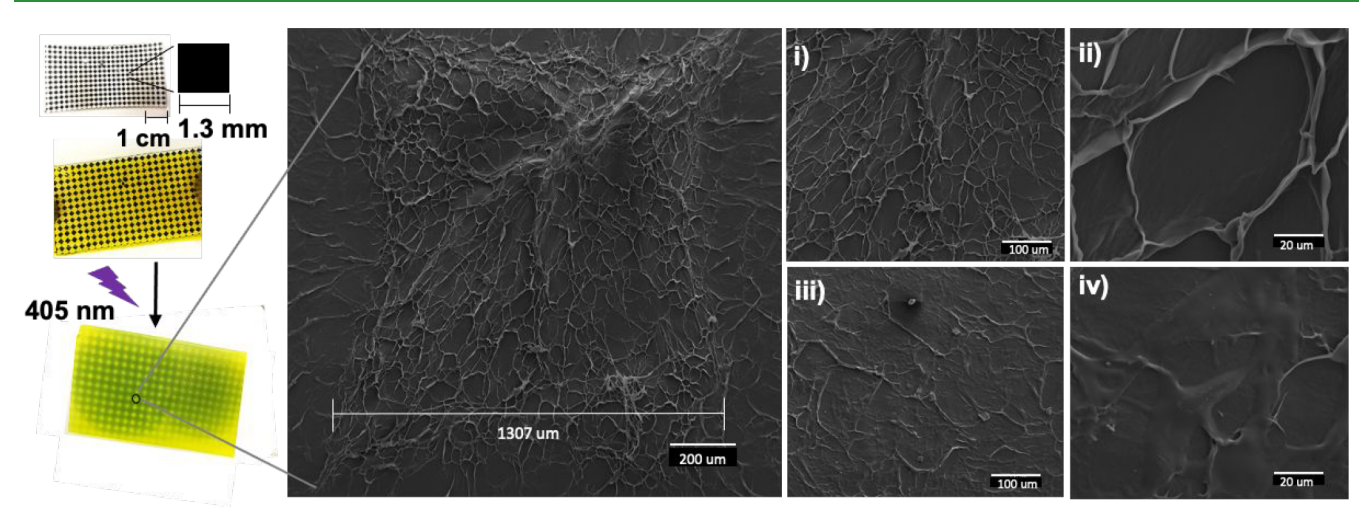


Figure 3. Photopatterning of an QHE-cellulose/agarose—V hydrogel. (A) The photomask with dark squares is kept on the hydrogel to design a photopattern. Dark-kept squares remain yellow, and irradiated areas turn green. (B) SEM micrographs of the photopatterned hydrogel showing the intact surface of a dark square at 70× magnification, where (i) and (ii) show the intact surface of the dark square at 150× and 1000× magnification, respectively, and (iii) and (iv) show the irradiated surface area at 150× and 1000× magnification, respectively.

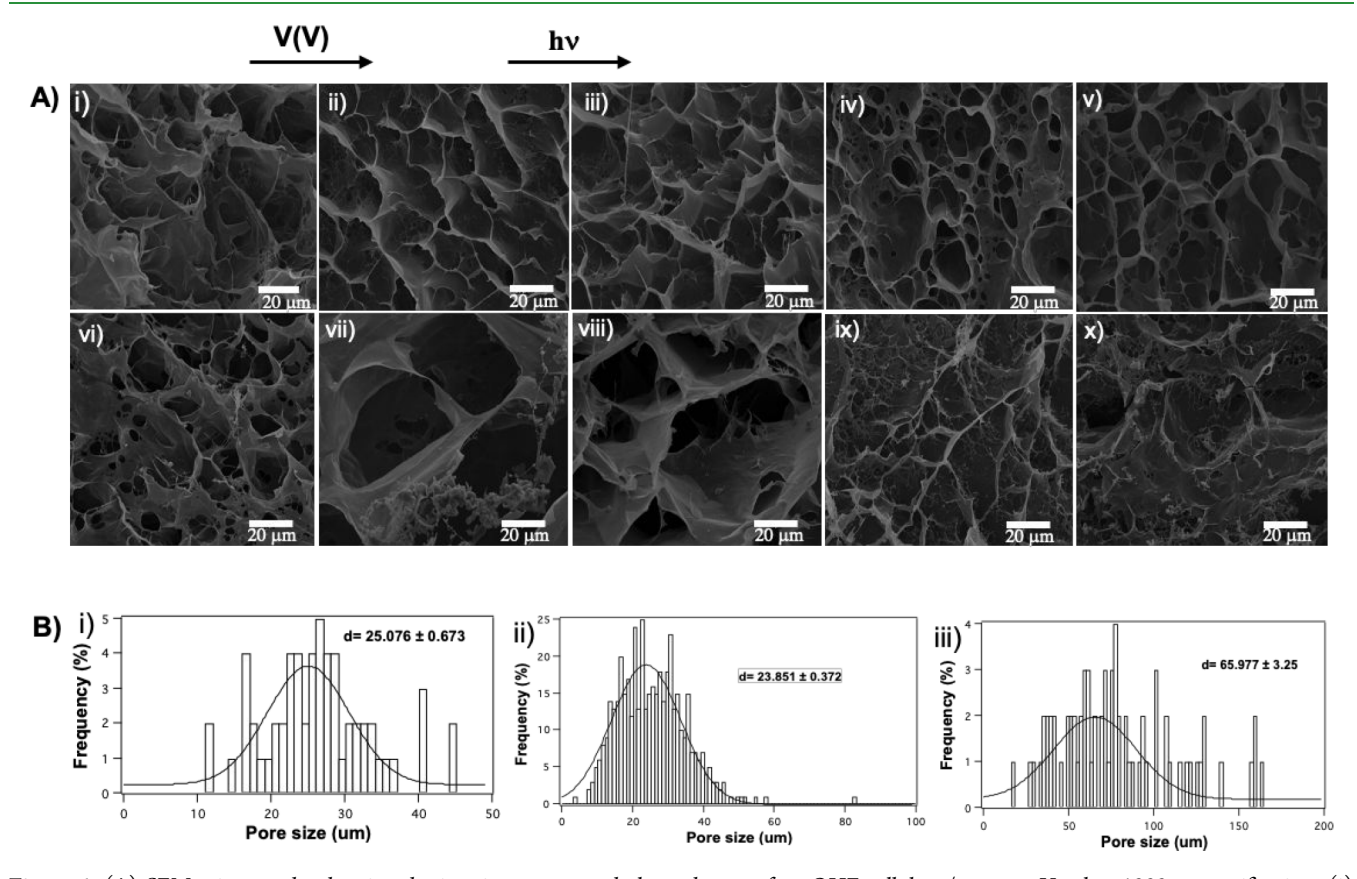


Figure 4. (A) SEM micrographs showing the interior pore morphology change of an QHE-cellulose/agarose—V gel at 1000× magnification: (i) QHE-cellulose/agarose gel (control); (ii) vanadium-coordinated gel before irradiation (dark); (iii) after 5 min of irradiation; (iv) after 30 min of irradiation; (v) after 60 min of irradiation; (vi) after 120 min of irradiation; (vii) gels showing maximum pore sizes after 180 min of irradiation; (viii) pores starting to collapse after 360 min of irradiation; (ix) collapsed pores after 720 min of irradiation; (x) collapsed pores after 1440 min of irradiation. (B) Histograms showing the average pore size distributions for the internal pores in the (i) control, (ii) dark, and (iii) 3 h irradiated hydrogels.

and smaller cavity formation was observed inside the pores, which connected to form larger cavities upon irradiation (Figure 4A). This was first observed in 30 min of irradiation (Figure 4A-iv) and gradually continued for 6 h of irradiation, where basic pore structure was still visible (Figure 4A-viii).

After exhaustive irradiation of the coordination hydrogel, the honeycomb structure was destroyed, and pores can be barely seen in 12 and 24 h irradiated gels (Figure 4A-ix,x). This was confirmed by analysis of the pore size distribution histograms and observation of each pore separately (Figures S10–S12).

Surface examination by SEM showed the gradual pore formation on the nonporous surface and irreversible changes in the surface texture upon irradiation (Figure S13). We thus used a simple photomask to create discrete patterns on these materials (Figure 3).

By measuring the changes in light absorption in the release medium above an 8 mm hydrogel disc, the release of V(IV) upon irradiation was monitored (Figures 5A and S14). The

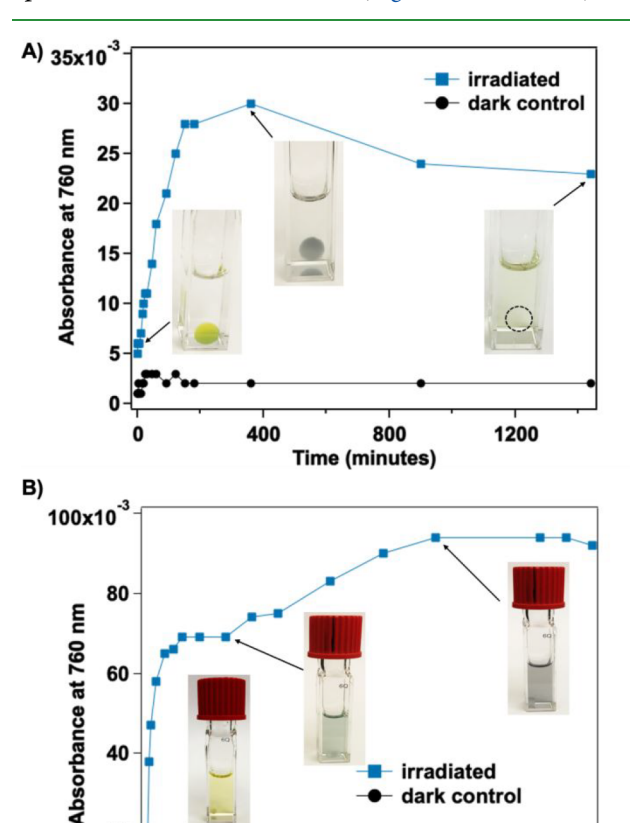


Figure 5. (A) Absorbance at 760 nm showing V(IV) formation in the release medium during irradiation of the gel disc. (B) Absorbance at 760 nm showing V(IV) formation upon irradiation of a QHEcellulose-V(V) solution. The black lines show changes in absorbance in the thermal control.

100

20

0

50

dark control

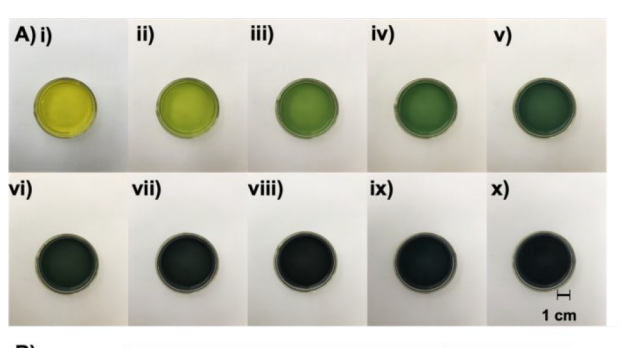
200

250

150

Time (minutes)

absorption spectrum of neat VO²⁺ shows an absorption maximum of 760 nm with a shoulder at 600 nm. 46,28 Gradual formation of V(IV) was observed as the absorbance at 760 nm increased. A continuous release of V(IV) as VO²⁺ was observed after up to 6 h of irradiation. Extensive reaction time, however, might result in the formation of other species, possibly oxidation of V(IV) to V(V) in the aqueous medium, which lowers the absorbance at 760 nm. A thermal control was maintained in the dark to show the very slow release of V(V) by thermal diffusion (Figure S14b). Similarly, an increase in the absorption at 760 nm was observed upon irradiation of the V(V)-coordinated QHE-cellulose solution (Figures 5B and S15). Formation of V(IV) upon irradiation was accompanied by the color change of the polysaccharide solution from yellow to blue (Figure 6A). A control experiment was maintained in the dark to show the presence of V(V) throughout the time of the experiment (Figure S15b).



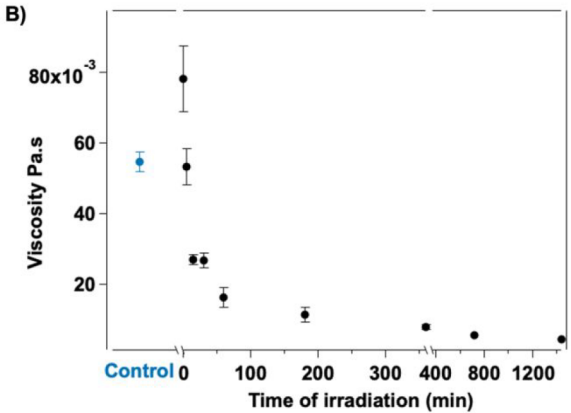


Figure 6. (A) Color changes of the QHE-cellulose-V(V) solution upon irradiation: (i) before irradiation (t = 0); (ii) t = 5 min of irradiation; (iii) t = 15 min of irradiation; (iv) t = 30 min of irradiation; (v) t = 60 min of irradiation; (vi) t = 120 min of irradiation; (vii) t = 180 min of irradiation; (viii) t = 360 min of irradiation; (ix) t = 720 min of irradiation; (x) t = 1440 min of irradiation. (B) Viscosity changes upon irradiation of the QHEcellulose-V(V) solution at 405 nm and 314 mW/cm². The control is the QHE-cellulose (polymer) solution without V coordination.

The effects of metal loading and irradiation on the rheological properties of the QHE-cellulose solution were studied through viscosity measurements (Figure 6). The viscosity of the polymer solution initially increased when the metal was introduced (Figure 6B). We attribute this to the V coordination, which creates the dynamic covalent cross-links in the hydrogel and thus a denser network. The viscosity of the polymer solution gradually decreased upon irradiation. This was attributed to breaking of the polysaccharide chains along with the reduction of V(V) to V(IV). The color change of the polymer solution (Figure 6A) was accompanied by the drop in the viscosity.

FTIR spectroscopy was used to identify the changes in the chemical composition of the hydrogels. FTIR spectra of the pure polymers, the QHE-cellulose/agarose hydrogel (control), the V-coordinated hydrogel, and the fully irradiated hydrogel (irradiated for 30 h and washed three times in deionized water) were compared. The signals of pure agarose (Figure 7Ai) dominated in the spectra of the control gels (Figure 7A-iii) and irradiated gels (Figure 7A-v). Characteristic absorption bands of agarose at 1643 cm⁻¹ (O-H bending), 1073 cm⁻¹ (C-O stretching vibrations), 933 cm⁻¹ (characteristic of 3,6anhydrogalactose), and 887 cm⁻¹ (C–H bending vibrations of anomeric carbon) corresponded with literature.⁴⁷ This indicates the absence of QHE-cellulose-V coordination in the fully irradiated gel. Agarose remains generally intact at the end, where QHE-cellulose itself is the sacrificial reductant in the photoreaction.

ACS Applied Bio Materials

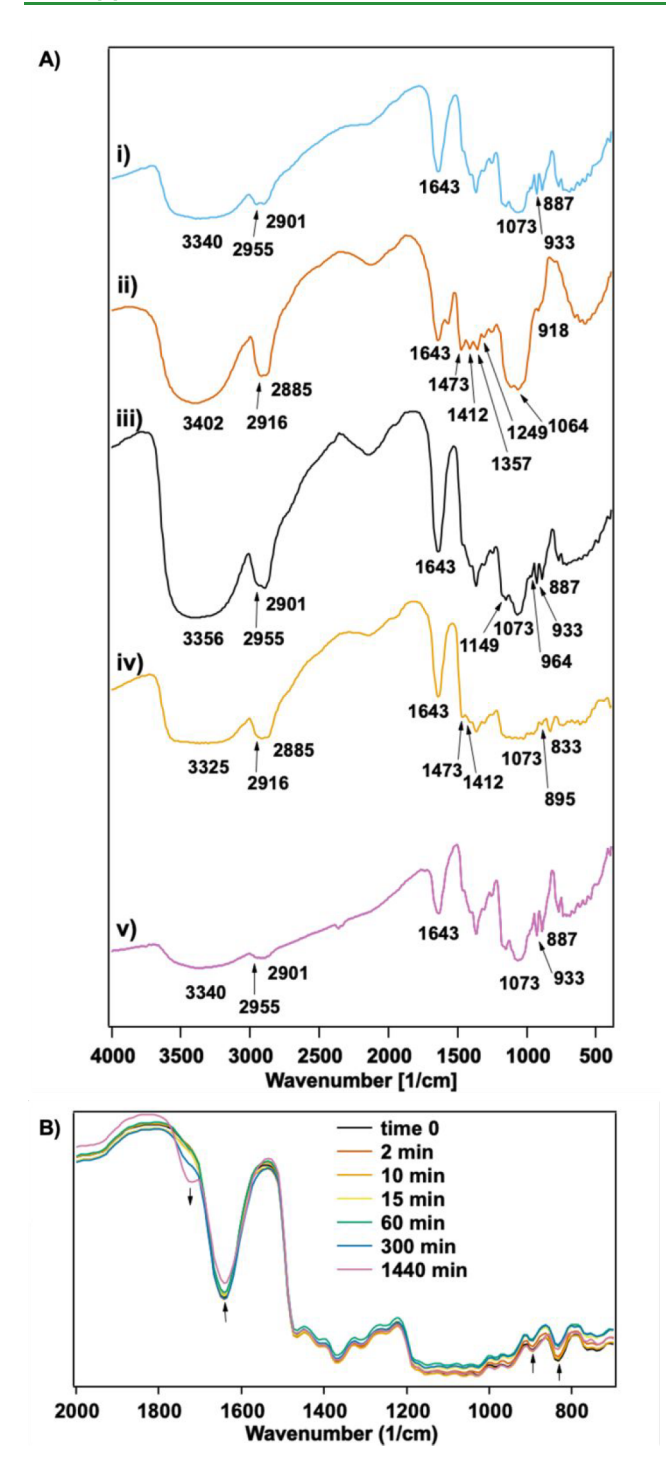


Figure 7. (A) FTIR spectra of (i) pure agarose, (ii) pure QHE-cellulose, (iii) QHE-cellulose/agarose hydrogel (control), (iv) QHE-cellulose/agarose—V(V)-coordinated hydrogel before irradiation, and (v) the fully irradiated hydrogel. (B) Evolution of the absorption bands upon irradiation of the QHE-cellulose/agarose—V(V)-coordinated hydrogel.

Characteristic absorption bands of QHE-cellulose (Figure 7A-ii) include a broad absorption at 3402 cm⁻¹ assigned to O—H stretching vibrations and medium absorption bands between 2916 and 2885 cm⁻¹ assigned to C—H stretching vibrations.⁴⁸ The absorption bands at 1473 and 1412 cm⁻¹ are assigned to O—H plane deformation of primary alcohol and C—H bending in —CHOH, respectively.³⁴ The absorption bands at 1357 and

1249 cm⁻¹ are assigned to the characteristic C-C and C-O vibrations of the cellulose skeleton.⁴⁹ The small, sharp band at 918 cm⁻¹ is assigned to the β -(1,4) glycosidic linkage.⁵⁰ The dark control (Figure 7A-iv) showed significant differences compared to the control gel (Figure 7A-iii), indicating vanadium coordination. The stretch at 1073 cm⁻¹, which can be attributed to the C-O-C vibration of the pyranose ring backbone, 51 showed much lower intensity in the dark control. Moreover, the stretch at 1149 cm⁻¹, which was attributed to the C-O antisymmetric vibration, 49 disappeared in the dark control. This is attributed to binding of vanadium to the ether oxygen in the polysaccharide ring. The broad absorption band at 3325 cm⁻¹ showed lower intensity, suggesting the binding of vanadium to the O-H region. A novel peak formation at 833 cm⁻¹ was seen only in the dark control, which was attributed to a V-O stretching mode, possibly in V-O-V or V-OH vibrations. 52,53 The intensity of this peak decreases upon irradiation (Figure 7B). The peak shift from 918 to 895 cm⁻¹ was attributed to vanadium coordination via the glycosidic linkage. The intensity of this peak also decreases upon irradiation, suggesting breaking of the glycosidic linkage (Figure 7B). The intensity of the stretch at 1643 cm⁻¹ also decreased, denoting a change in vanadium coordination with O-H stretches. A novel peak formation at 1720 cm⁻¹ possibly denoted the formation of C=O stretch in an acetal formed from the oxidation of the QHE-cellulose, as seen in the NMR spectrum upon irradiation (Figure S23). Peaks at 1473 and 948 cm⁻¹ correspond to bending and stretching vibrations of quaternary ammonium groups.44

Hydrogels are widely applied as intelligent carriers in controlled drug delivery systems. 54,55 When a molecule is bulky enough to be trapped inside, photostable, and nonreactive with other components, this can be chosen as a guest cargo for the hydrogel beads based on the charge and the steric bulk. 16 According to this approach, photorelease of guest cargo from the agarose/QHE-cellulose-V beads was studied using a drug-model compound, folic acid. The absorbance of the release medium above the loaded beads was measured after each irradiation (Figure 8A). The increase in absorbance at 268 nm with time implied the photorelease of the encapsulated cargo (Figure 8B). The dark control showed only a slight release by thermal diffusion (Figure S16). We attribute the color change of the beads from yellow to green to the reduction from V(V) to V(IV) as discussed above. Possible breakdown of QHE-cellulose chains and changes in the coordination interaction cause rupturing of the beads, which triggers the release of the encapsulated folic acid cargo as well as V(IV). The efficiency of this system was higher than that of the previously studied Fe(III)-polyuronic acid-coordinated hydrogel system, with ~75% release of folic acid observed after 6 h of irradiation time (314 mW/cm²) for the V gels compared to 75% release after 60 h of irradiation time (50 mW/cm²) for the Fe(III) gels. 16 The loaded beads were mechanically and chemically stable, hosting the cargo for long periods of time (Figure S16).

Thermogravimetric analysis was carried out on hydrogels during the photochemical treatment to study the thermal stability and ceramic yield (Figures 9 and S17). An initial endothermic loss (12–15%) of superficial water and other volatile matter occurred between 25 and 200 °C for all of the samples. Control agarose/QHE-cellulose gels (Figure S17c) showed two distinct degradation transitions related to the equal contribution of pure polymers (Figure S17a,b). This

ACS Applied Bio Materials www.acsabm.org Article

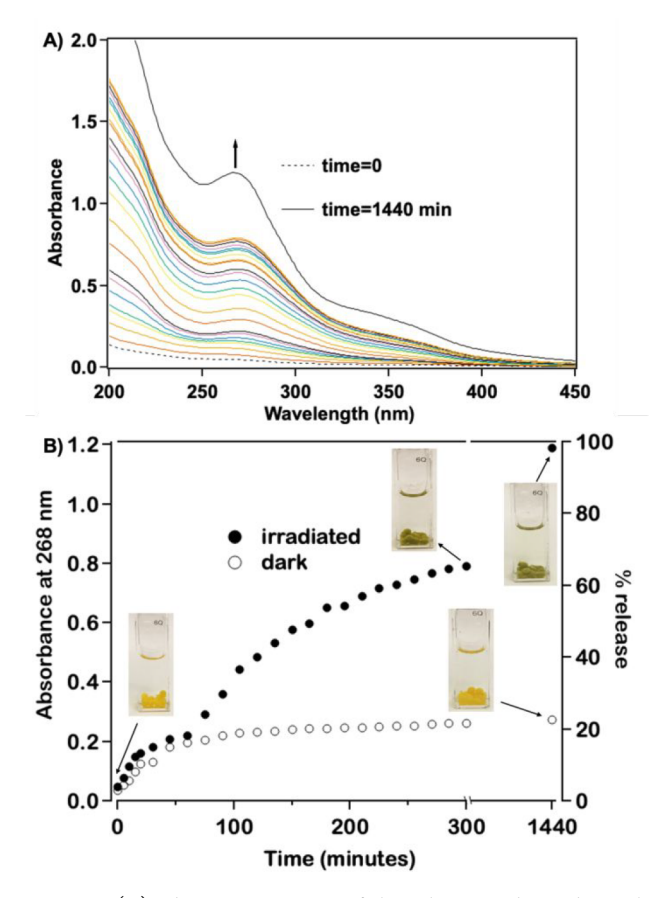
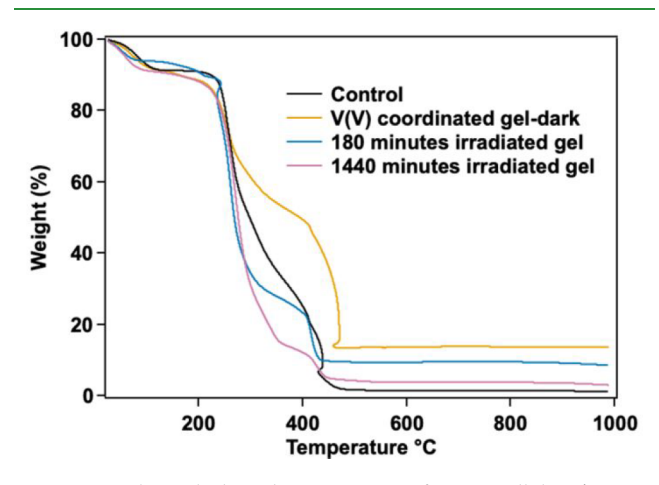


Figure 8. (A) Absorption spectra of the release medium above the folic acid-encapsulated gel beads upon irradiation at 405 nm and 314 mW/cm². (B) Absorbance at 268 nm plotted vs time to show the release profile (solid circles) and images of the beads upon irradiation. The thermal control (open circles) did not show the same increase in absorbance.



 $\label{eq:Figure 9.} \textbf{Figure 9.} \ \ \text{Thermal degradation curves of QHE-cellulose/agarose} \ \ \text{hydrogels with different treatments.} \ \ \text{The control is the QHE-cellulose/agarose} \ \ \text{hydrogel without V coordination.}$

total weight loss (\sim 84%) was attributed to the decomposition of the polysaccharide chains. ²⁹ An increase in the thermal stability was observed upon coordination of the metal with polymer chains. For the V(V)-coordinated gel (Figure S17d), the second and third degradations at 251 and 424 °C appeared at higher temperatures than those of the control. Furthermore, the largest weight loss in the third degradation was observed

only in the V(V)-coordinated gel. The third degradation was strongly exothermic, and a lower rate of degradation was noted after the inflection point. We attribute these to stabilization of the QHE-cellulose component by the metal. However, the third degradation step maximum decreased relative to the second degradation step upon irradiation (Figure S17e,f, not on the same scale). Hence, the third degradation step was attributed to the decomposition of the V-QHE-cellulose bonds. The third-degradation-step transitions at 415 and 420 °C for gels irradiated for 3 and 24 h, respectively, appeared at lower temperatures than for the dark control. This indicated a lower thermal stability of V-QHE-cellulose coordination upon irradiation. The degradation pattern of the gel irradiated for 24 h (Figure S17f) was correlated to that of the control gel (Figure S17c) with a smaller contribution from the cellulose component. Hence, the second degradation transition at around 250 °C was attributed to the decomposition of agarose chains. TGA was also a useful diagnostic tool to calculate the percentage of nonignitable minerals, possibly as residual vanadium oxides (V_xO_y) after the thermal degradation. The control gel was completely burned off with no ceramic yield, whereas the dark gel remained with a 13% ceramic yield, as expected due to the presence of the V in the dark material that is not in the control gel. After irradiation, the ceramic yield decreased with increasing irradiation time (3 h irradiation, 8% ceramic yield; 24 h irradiation, 3% ceramic yield). This indicates the gradual leaching of V out of the gel upon irradiation.

Inductively coupled plasma optical emission spectroscopy was carried out to confirm the gradual leaching of vanadium out of the gels upon irradiation. The vanadium content in the hydrogels gradually decreased, and almost total removal of the metal ion was observed after 24 h of irradiation (Figures 10 and S9a). We correlate the removal of the metal with the increase in pore diameter primarily after 120 min of irradiation (Figure 10). However, during the first 120 min of irradiation, the vanadium content in the gels does not decrease with the

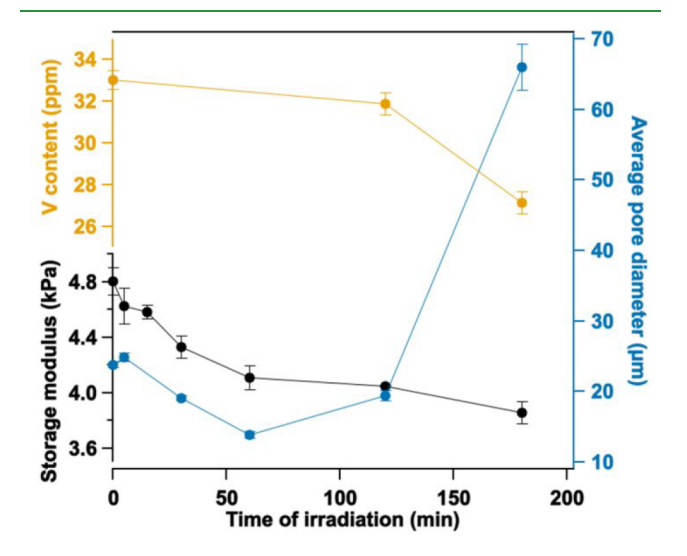


Figure 10. Changes in storage modulus, average pore diameter as measured by SEM and ImageJ, and V content (in ppm) upon irradiation (405 nm and 314 mW/cm²) of QHE-cellulose/agarose–V hydrogels. Up to 3 h of irradiation was considered for this plot because exhaustive irradiation caused destruction of the pore structure. Changes in storage modulus and V content through 24 h of irradiation are presented in Figure S9.

storage modulus (Figure 10). Hence, the initial drop in mechanical properties is perhaps due to the reduction of vanadium and degradation of cellulose within the hydrogel matrix. Further degradation of the polysaccharide matrix was accompanied by exhaustive irradiation and removal of metal ions (Figure S9b). Vanadium concentrations as obtained by the analysis are stated in Table S3.

The color change of the QHE-cellulose/agarose-V(V) hydrogel upon irradiation was characterized by diffuse reflectance spectroscopy and UV-vis spectroscopy (Figure S18). In diffuse reflectance spectroscopy, the percentage reflection of the colored material upon each irradiation was monitored. The complete color profile of the QHE-cellulose/ agarose-V hydrogel strip is provided in Figure S19. A minimum (nadir) in the percentage reflection at 450 nm indicated the yellow color of the hydrogel before irradiation. An increase in the percentage reflection was observed at 450 nm when the hydrogel turned blue. The formation of a broad peak was observed at around 700 nm when the hydrogel turned green, and the peak was slightly blue-shifted when the gel turned blue (Figure S18). The percentage reflection minima and peaks match with the complementary colors of the hydrogel, which agrees with the absorbance spectra (Figure S18b). The R, G, B color analysis was done for the QHEcellulose-V solutions shown in Figure 6A. Analysis carried out with the ImageI software confirmed the decrease in the R and G values and the increase in the B value during irradiation (Figure S20). The calculated R, G, B values were consistent with the color differences of the polymer solution (Table S2).

The hydrophilic groups and repulsion between negatively charged carboxylic groups cause expansion of polymer coils and increase the osmotic pressure in the gel, which results in swelling. 43 The swelling behavior and transport dynamics of these hydrogels were studied in dynamic swelling experiments at different irradiation times. Five hydrogel discs with a diameter of 8 mm (n = 5) were studied for each irradiation (Figure S21a). The swelling capacity of the gels decreased with irradiation (Figure S21c). This can be attributed to the lower osmotic pressure and lower expansion of polymer coils upon irradiation. The degradation of the cellulose segment and leaching of oligomers can result in a material with lower hydrophilicity and a lower capacity to absorb water. The continued loss of dry weight upon irradiation validates this observation (Figure S22). However, when the metal was reoxidized, the swelling capacity slightly increased when V(V)-cellulose coordination retained some hydrogen-bonding sites (Figure S21b).

CONCLUSIONS

We were able to show the introduction of V(V) coordination cross-links into polymer hydrogels to create photoresponsiveness. Properties of the hydrogel were tuned during light irradiation when V(V) was photoreduced to V(IV) with consecutive oxidation of the polymer matrix. We have used these hydrogels for controlled delivery of V(IV) and/or encapsulated cargo. The possibility to pattern the mechanical properties of the substrate is an incentive due to the responsiveness of these systems. Just by controlling the exposure to light, mechanical properties of the matrix as well as the strength of V coordination were manipulated. Light was used to create discrete patterns on these materials as gradients in elasticity and flow properties. By photopatterning, we have created mechanical grooves to code the functionality of the

hydrogel. Similar to our previously reported Fe(III)-coordinated hydrogels, ¹⁶ we expect these materials to find application in a variety of systems where photopatterning of the mechanical properties or degradation of the hydrogel is needed.

ASSOCIATED CONTENT

Supporting Information

The Supporting Information is available free of charge at https://pubs.acs.org/doi/10.1021/acsabm.2c00529.

Chemical structures, pH studies, storage and loss modulus values, UV-vis spectra, TGA spectra, diffuse reflectance spectra, RGB analysis, vanadium concentrations as obtained by ICP/OES analysis, swelling studies, dry weight analysis, NMR spectra, pore diameter histograms, SEM images, and pictures of color changes of gels and solutions (PDF)

AUTHOR INFORMATION

Corresponding Author

Alexis D. Ostrowski — Department of Chemistry and Center for Photochemical Sciences, Bowling Green State University, Bowling Green, Ohio 43403, United States; oorcid.org/0000-0002-3207-1845; Email: alexiso@bgsu.edu

Authors

E. A. Kalani D. Edirisinghe – Department of Chemistry and Center for Photochemical Sciences, Bowling Green State University, Bowling Green, Ohio 43403, United States

Carina Haddad – Department of Chemistry and Center for Photochemical Sciences, Bowling Green State University, Bowling Green, Ohio 43403, United States

Complete contact information is available at: https://pubs.acs.org/10.1021/acsabm.2c00529

Author Contributions

The manuscript was written through contributions of all authors. All of the authors approved the final version of the manuscript.

Notes

The authors declare no competing financial interest.

ACKNOWLEDGMENTS

We thank Dr. Marilyn Cayer (Microscopy and Imaging Facility, Bowling Green State University) for assistance with SEM imaging, Dr. Joseph C. Furgal (Bowling Green State University) for help and advice on TGA, and Dr. John Farver (School of Earth, Environment and Society, Bowling Green State University) for the help and advice with ICP-OES studies. We thank the NSF CAREER Program and the Chemistry CSDM-B and DMR Polymers Programs for funding (CHE-1653892). We also acknowledge the generous support of the Thomas J. Kinstle Professorship at BGSU.

ABBREVIATIONS

QHE-cellulose, quaternized hydroxyethyl cellulose ethoxylate; SEM, scanning electron microscopy; TGA, thermogravimetric analysis; UV-vis, ultraviolet-visible spectroscopy; ICP-OES, inductively coupled plasma optical emission spectroscopy; NMR, nuclear magnetic resonance spectroscopy; FTIR, Fourier transform infrared spectroscopy; LED, light-emitting diode

REFERENCES

- (1) Akter, M.; Bhattacharjee, M.; Dhar, A. K.; Rahman, F. B. A.; Haque, S.; Rashid, T. U.; Kabir, S. M. F. Cellulose-Based Hydrogels for Wastewater Treatment: A Concise Review. *Gels* **2021**, *7* (1), 30.
- (2) Sinha, V.; Chakma, S. Advances in the Preparation of Hydrogel for Wastewater Treatment: A Concise Review. *J. Environ. Chem. Eng.* **2019**, *7* (5), 103295.
- (3) Giammanco, G. E.; Carrion, B.; Coleman, R. M.; Ostrowski, A. D. Photoresponsive Polysaccharide-Based Hydrogels with Tunable Mechanical Properties for Cartilage Tissue Engineering. *ACS Appl. Mater. Interfaces* **2016**, 8 (23), 14423–14429.
- (4) Jin, R.; Dijkstra, P. J. Hydrogels for Tissue Engineering Applications. In *Biomedical Applications of Hydrogels Handbook*; Ottenbrite, R. M., Park, K., Okano, T., Eds.; Springer: New York, 2010; pp 203–225. DOI: 10.1007/978-1-4419-5919-5 11.
- (5) Burdick, J. A.; Murphy, W. L. Moving from Static to Dynamic Complexity in Hydrogel Design. *Nat. Commun.* **2012**, 3 (1), 1269.
- (6) Sun, J.; Tan, H. Alginate-Based Biomaterials for Regenerative Medicine Applications. *Materials* **2013**, *6* (4), 1285–1309.
- (7) Linsley, C. S.; Wu, B. M. Recent Advances in Light-Responsive on-Demand Drug-Delivery Systems. *Ther. Delivery* **2017**, 8 (2), 89–107.
- (8) Vashist, A.; Vashist, A.; Gupta, Y. K.; Ahmad, S. Recent Advances in Hydrogel Based Drug Delivery Systems for the Human Body. *J. Mater. Chem. B* **2014**, *2* (2), 147–166.
- (9) Lee, Y.; Song, W. J.; Sun, J.-Y. Hydrogel Soft Robotics. *Mater. Today Phys.* **2020**, *15*, 100258.
- (10) Banerjee, H.; Suhail, M.; Ren, H. Hydrogel Actuators and Sensors for Biomedical Soft Robots: Brief Overview with Impending Challenges. *Biomimetics* **2018**, 3 (3), 15.
- (11) Wang, W.; Narain, R.; Zeng, H. Chapter 10: Hydrogels. In *Polymer Science and Nanotechnology*; Narain, R., Ed.; Elsevier, 2020; pp 203–244. DOI: 10.1016/B978-0-12-816806-6.00010-8.
- (12) Dong, H.; Snyder, J. F.; Williams, K. S.; Andzelm, J. W. Cation-Induced Hydrogels of Cellulose Nanofibrils with Tunable Moduli. *Biomacromolecules* **2013**, *14* (9), 3338–3345.
- (13) Liu, X.; Zhong, M.; Shi, F.; Xu, H.; Xie, X. Multi-Bond Network Hydrogels with Robust Mechanical and Self-Healable Properties. *Chin. J. Polym. Sci.* **2017**, *35* (10), 1253–1267.
- (14) Grindy, S. C.; Holten-Andersen, N. Bio-Inspired Metal-Coordinate Hydrogels with Programmable Viscoelastic Material Functions Controlled by Longwave UV Light. *Soft Matter* **2017**, *13* (22), 4057–4065.
- (15) Haddad, C.; Edirisinghe, E. A. K. D.; Brown, H. M.; Ostrowski, A. D. Photoreactivity and Enhanced Mechanical Properties and Water Stability in Polysaccharide-Based Films Using Vanadium Ion Coordination. ACS Appl. Polym. Mater. 2022, 4 (2), 859–867.
- (16) Giammanco, G. E.; Sosnofsky, C. T.; Ostrowski, A. D. Light-Responsive Iron(III)-Polysaccharide Coordination Hydrogels for Controlled Delivery. ACS Appl. Mater. Interfaces 2015, 7 (5), 3068–3076.
- (17) Giammanco, G. E.; Ostrowski, A. D. Photopatterning the Mechanical Properties of Polysaccharide-Containing Gels Using Fe³⁺ Coordination. *Chem. Mater.* **2015**, 27 (14), 4922–4925.
- (18) Davis, J. M. Oxidation States of Vanadium. *J. Chem. Educ.* **1968**, 45 (7), 473.
- (19) Skyllas-Kazacos, M.; Kazacos, M. State of Charge Monitoring Methods for Vanadium Redox Flow Battery Control. *J. Power Sources* **2011**, 196 (20), 8822–8827.
- (20) Park, J. P.; Song, I. T.; Lee, J.; Ryu, J. H.; Lee, Y.; Lee, H. Vanadyl-Catecholamine Hydrogels Inspired by Ascidians and Mussels. *Chem. Mater.* **2015**, *27* (1), 105–111.
- (21) Pessoa, J. C.; Etcheverry, S.; Gambino, D. Vanadium Compounds in Medicine. *Coord. Chem. Rev.* **2015**, *301*, 24–48.
- (22) Treviño, S.; Díaz, A.; Sánchez-Lara, E.; Sanchez-Gaytan, B. L.; Perez-Aguilar, J. M.; González-Vergara, E. Vanadium in Biological Action: Chemical, Pharmacological Aspects, and Metabolic Implications in Diabetes Mellitus. *Biol. Trace Elem. Res.* **2019**, *188* (1), 68–98.

- (23) Alvarez-Lorenzo, C.; Blanco-Fernandez, B.; Puga, A. M.; Concheiro, A. Crosslinked Ionic Polysaccharides for Stimuli-Sensitive Drug Delivery. *Adv. Drug Delivery Rev.* **2013**, *65* (9), 1148–1171.
- (24) Kremer, L. E.; McLeod, A. I.; Aitken, J. B.; Levina, A.; Lay, P. A. Vanadium(V) and -(IV) Complexes of Anionic Polysaccharides: Controlled Release Pharmaceutical Formulations and Models of Vanadium Biotransformation Products. *J. Inorg. Biochem.* **2015**, *147*, 227–234.
- (25) Pianowski, Z. L. Recent Implementations of Molecular Photoswitches into Smart Materials and Biological Systems. *Chem. Eur. J.* **2019**, 25 (20), 5128–5144.
- (26) Zhou, F.; Wu, S.; Rader, C.; Ma, J.; Chen, S.; Yuan, X.; Foster, E. J. Crosslinked Ionic Alginate and Cellulose-Based Hydrogels for Photoresponsive Drug Release Systems. *Fibers Polym.* **2020**, *21* (1), 45–54
- (27) Brega, V.; Scaletti, F.; Zhang, X.; Wang, L.-S.; Li, P.; Xu, Q.; Rotello, V. M.; Thomas, S. W. Polymer Amphiphiles for Photoregulated Anticancer Drug Delivery. *ACS Appl. Mater. Interfaces* **2019**, *11* (3), 2814–2820.
- (28) Edirisinghe, E. A. K. D.; Ayodele, M. J.; Saeedi, S.; Brugh, A. M.; Forbes, M. D. E.; White, T. A.; Ostrowski, A. D. Reversible Photochemistry in Vanadium(V) Tartrate Clusters Containing a Mixed-Valent Intermediate. *Inorg. Chem.* 2022, submitted.
- (29) Su, T.; Zhang, M.; Zeng, Q.; Pan, W.; Huang, Y.; Qian, Y.; Dong, W.; Qi, X.; Shen, J. Mussel-Inspired Agarose Hydrogel Scaffolds for Skin Tissue Engineering. *Bioact. Mater.* **2021**, *6* (3), 579–588.
- (30) Cao, Z.; Gilbert, R. J.; He, W. Simple Agarose-Chitosan Gel Composite System for Enhanced Neuronal Growth in Three Dimensions. *Biomacromolecules* **2009**, *10* (10), 2954–2959.
- (31) Gallagher, Z. J.; Fleetwood, S.; Kirley, T. L.; Shaw, M. A.; Mullins, E. S.; Ayres, N.; Foster, E. J. Heparin Mimic Material Derived from Cellulose Nanocrystals. *Biomacromolecules* **2020**, *21* (3), 1103–1111.
- (32) Xu, F. J.; Zhu, Y.; Liu, F. S.; Nie, J.; Ma, J.; Yang, W. T. Comb-Shaped Conjugates Comprising Hydroxypropyl Cellulose Backbones and Low-Molecular-Weight Poly(N-Isopropylacryamide) Side Chains for Smart Hydrogels: Synthesis, Characterization, and Biomedical Applications. *Bioconjugate Chem.* **2010**, *21* (3), 456–464.
- (33) Peng, B.; Yao, Z.; Wang, X.; Crombeen, M.; Sweeney, D. G.; Tam, K. C. Cellulose-Based Materials in Wastewater Treatment of Petroleum Industry. *Green Energy Environ.* **2020**, *5* (1), 37–49.
- (34) Jilal, I.; El Barkany, S.; Bahari, Z.; Sundman, O.; El Idrissi, A.; Abou-Salama, M.; Romane, A.; Zannagui, C.; Amhamdi, H. New Quaternized Cellulose Based on Hydroxyethyl Cellulose (HEC) Grafted EDTA: Synthesis, Characterization and Application for Pb (II) and Cu (II) Removal. *Carbohydr. Polym.* **2018**, *180*, 156–167.
- (35) Liu, L.; Gao, Z. Y.; Su, X. P.; Chen, X.; Jiang, L.; Yao, J. M. Adsorption Removal of Dyes from Single and Binary Solutions Using a Cellulose-Based Bioadsorbent. *ACS Sustain. Chem. Eng.* **2015**, 3 (3), 432–442.
- (36) Mishra, R. K.; Ramasamy, K.; Ban, N. N.; Majeed, A. B. A. Synthesis of Poly[3-(Methacryloylamino) Propyl Trimethylammonium Chloride- *Co*-Methacrylic Acid] Copolymer Hydrogels for Controlled Indomethacin Delivery. *J. Appl. Polym. Sci.* **2013**, *128* (5), 3365–3374.
- (37) Wei, W.; Qi, X.; Li, J.; Zhong, Y.; Zuo, G.; Pan, X.; Su, T.; Zhang, J.; Dong, W. Synthesis and Characterization of a Novel Cationic Hydrogel Base on Salecan-g-PMAPTAC. *Int. J. Biol. Macromol.* **2017**, *101*, 474–480.
- (38) Tang, Z.; Deng, W.; Wang, Y.; Zhu, E.; Wan, X.; Zhang, Q.; Wang, Y. Transformation of Cellulose and Its Derived Carbohydrates into Formic and Lactic Acids Catalyzed by Vanadyl Cations. *ChemSusChem* **2014**, *7* (6), 1557–1567.
- (39) Niu, M.; Hou, Y.; Wu, W.; Ren, S.; Yang, R. Successive C1-C2 Bond Cleavage: The Mechanism of Vanadium(v)-Catalyzed Aerobic Oxidation of d-Glucose to Formic Acid in Aqueous Solution. *Phys. Chem. Chem. Phys.* **2018**, *20* (26), 17942–17951.

- (40) Rinaudo, M. Main Properties and Current Applications of Some Polysaccharides as Biomaterials. *Polym. Int.* **2008**, *57* (3), 397–430
- (41) Shukla, N. B.; Rattan, S.; Madras, G. Swelling and Dye-Adsorption Characteristics of an Amphoteric Superabsorbent Polymer. *Ind. Eng. Chem. Res.* **2012**, *51* (46), 14941–14948.
- (42) Tang, S. C. N.; Lo, I. M. C.; Mak, M. S. H. Comparative Study of the Adsorption Selectivity of Cr(VI) onto Cationic Hydrogels with Different Functional Groups. *Water. Air. Soil Pollut.* **2012**, 223 (4), 1713–1722.
- (43) Kabir, S. M. F.; Sikdar, P. P.; Haque, B.; Bhuiyan, M. A. R.; Ali, A.; Islam, M. N. Cellulose-Based Hydrogel Materials: Chemistry, Properties and Their Prospective Applications. *Prog. Biomater.* **2018**, 7 (3), 153–174.
- (44) Qi, X.; Li, J.; Wei, W.; Zuo, G.; Su, T.; Pan, X.; Zhang, J.; Dong, W. Cationic Salecan-Based Hydrogels for Release of 5-Fluorouracil. RSC Adv. 2017, 7 (24), 14337–14347.
- (45) Gomez-Hermoso-de-Mendoza, J.; Barud, H. S.; Gutierrez, J.; Tercjak, A. Flexible Photochromic Cellulose Triacetate Based Bionanocomposites Modified with Sol-Gel Synthesized V₂O₅ Nanoparticles. *Carbohydr. Polym.* **2019**, 208, 50–58.
- (46) Roznyatovskaya, N.; Herr, T.; Küttinger, M.; Fühl, M.; Noack, J.; Pinkwart, K.; Tübke, J. Detection of Capacity Imbalance in Vanadium Electrolyte and Its Electrochemical Regeneration for All-Vanadium Redox-Flow Batteries. *J. Power Sources* **2016**, 302, 79–83.
- (47) Hu, Z.; Hong, P.; Liao, M.; Kong, S.; Huang, N.; Ou, C.; Li, S. Preparation and Characterization of Chitosan-Agarose Composite Films. *Materials* **2016**, *9* (10), 816.
- (48) Azzaoui, K.; Mejdoubi, E.; Lamhamdi, A.; Zaoui, S.; Berrabah, M.; Elidrissi, A.; Hammouti, B.; Fouda, M. M. G.; Al-Deyab, S. S. Structure and Properties of Hydroxyapatite/Hydroxyethyl Cellulose Acetate Composite Films. *Carbohydr. Polym.* **2015**, *115*, 170–176.
- (49) El Idrissi, A.; El Barkany, S.; Amhamdi, H.; Maaroufi, A.-K. Physicochemical Characterization of Celluloses Extracted from Esparto "Stipa Tenacissima" of Eastern Morocco. *J. Appl. Polym. Sci.* **2013**, *128* (1), 537–548.
- (50) Sun, R.; Sun, X.; Liu, G.; Fowler, P.; Tomkinson, J. Structural and Physicochemical Characterization of Hemicelluloses Isolated by Alkaline Peroxide from Barley Straw. *Polym. Int.* **2002**, *51* (2), 117–124.
- (51) Huang, S.; Wang, X.; Shen, J.; Wu, R.; Zhao, H.; Wang, Y.; Wang, Y.; Xia, Y. Surface Functionalization of Cellulose Nanocrystals with Polymeric Ionic Liquids during Phase Transfer. *Carbohydr. Polym.* **2017**, *157*, 1426–1433.
- (52) Wang, T.; Liu, X.; Ma, C.; Wei, M.; Huo, P.; Yan, Y. In Situ Construction of BiVO4(–)Cellulose Fibers@CDs(–)Polyvinyl Alcohol Composites for Tetracycline Photocatalytic Degradation. *Sci. China Technol. Sci.* **2021**, *64* (3), 548–558.
- (53) Guimond, S.; Abu Haija, M.; Kaya, S.; Lu, J.; Weissenrieder, J.; Shaikhutdinov, S.; Kuhlenbeck, H.; Freund, H.-J.; Döbler, J.; Sauer, J. Vanadium Oxide Surfaces and Supported Vanadium Oxide Nanoparticles. *Top. Catal.* **2006**, *38* (1), 117–125.
- (54) Peppas, N. A.; Hilt, J. Z.; Khademhosseini, A.; Langer, R. Hydrogels in Biology and Medicine: From Molecular Principles to Bionanotechnology. *Adv. Mater.* **2006**, *18* (11), 1345–1360.
- (55) Liao, S. W.; Rawson, J.; Omori, K.; Ishiyama, K.; Mozhdehi, D.; Oancea, A. R.; Ito, T.; Guan, Z.; Mullen, Y. Maintaining Functional Islets through Encapsulation in an Injectable Saccharide-Peptide Hydrogel. *Biomaterials* **2013**, *34* (16), 3984–3991.

☐ Recommended by ACS

Multifunctional Hybrid Nanocomposite Hydrogel Releasing Different Biomolecular Species Triggered with Different Biochemical Signals Processed by Orthogonal Biocatalytic...

Ronaldo Badenhorst, Oleh Smutok, et al.

DECEMBER 05, 2022

ACS APPLIED BIO MATERIALS

READ 🗹

Synthesis, Characterization, and Digital Light Processing of a Hydrolytically Degradable Hyaluronic Acid Hydrogel

Jonathan H. Galarraga, Jason A. Burdick, et al.

DECEMBER 14, 2022

BIOMACROMOLECULES

READ 🗹

Tuning the Mechanical Properties of Multiarm RAFT-Based Block Copolyelectrolyte Hydrogels *via* Ionic Cross-Linking for 3D Cell Cultures

Duyen H. T. Nguyen, J. Justin Gooding, et al.

DECEMBER 13, 2022

BIOMACROMOLECULES

READ **C**

Enzymatically Triggered Deprotection and Cross-Linking of Thiolated Alginate-Based Bioinks

Sajjad Naeimipour, Daniel Aili, et al.

OCTOBER 21, 2022

CHEMISTRY OF MATERIALS

READ 🗹

Get More Suggestions >